



Mohammad Reza Oshaghi · Hossein Afshin ·
Bahar Firoozabadi

Investigation of bubble formation and its detachment in shear-thinning liquids at low capillary and Bond numbers

Received: 23 December 2018 / Accepted: 13 August 2019 / Published online: 21 August 2019
© Springer-Verlag GmbH Germany, part of Springer Nature 2019

Abstract In the present paper, the formation of an air bubble in a shear-thinning non-Newtonian fluid was investigated numerically. For modeling, an algebraic volume of fluid (VOF) solver of OpenFOAM[®] was improved by applying a Laplacian filter and was evaluated using the experimental results from the literature. The enhanced solver could compute the surface tension force more accurately, and it was important especially at low capillary and Bond numbers due to the dominance of surface tension force relative to the other forces. The adiabatic bubble growth was simulated in an axisymmetric domain for $Bo = 0.05, 0.1, 0.5$ and $Ca = 10^{-1}, 10^{-2}, 10^{-3}, 10^{-4}$, and the bubble detachment time and volume were examined. According to the results, for Newtonian fluids, there is a critical capillary number for a given Bond number, and for lower values of this critical number, no difference is observed between the bubble detachment volumes and also bubble detachment times. Similarly, the results indicated that for non-Newtonian fluids, if apparent capillary number (obtained by apparent viscosity) is less than the critical capillary number, the detachment volume is the same as the corresponding Newtonian case. The velocity of the bubble during its formation in Newtonian and shear-thinning fluids was also studied. Moreover, the bubble formation and detachment characteristics such as instantaneous contact angle and necking radius were investigated for Newtonian and non-Newtonian liquids, and the shear-thinning effect was examined as well. The results indicated that changing the ambient fluid to a non-Newtonian liquid has no effect on the trend of the contact angle; however, the minimum contact angle has a higher value when the shear-thinning effect increases. Also, the variation of neck radius with the time until detachment was presented by the power relation $R_n = (t_{det} - t)^\eta$, and the effect of shear thinning on its exponent η was investigated.

Keywords Bubble formation · Shear-thinning fluid · Neck radius · OpenFOAM · VOF

1 Introduction

Bubble formation from an orifice submerged in non-Newtonian fluids has many applications in chemical industries such as bubble reactors, wastewater treatment, fermentations, composites and plastic foam processing,

Communicated by Tim Phillips.

M. R. Oshaghi · H. Afshin (✉) · B. Firoozabadi
School of Mechanical Engineering, Sharif University of Technology, Tehran, Iran
E-mail: Afshin@sharif.edu

M. R. Oshaghi
E-mail: oshaghi@mech.sharif.ir

B. Firoozabadi
E-mail: firoozabadi@sharif.edu

and polymer devolatilization. In most of them, the ambient liquid is a non-Newtonian fluid. Determining the bubble formation behavior is essential for the optimal design of gas–liquid equipment, and thus, the study of bubble formation has received great attention [1,2].

Bubble formation at submerged orifices can be categorized into three bubble regimes: static, dynamic, and turbulent. At very low flow rates, the static regime occurs where the inertial and viscous forces can be neglected. In this regime, the bubble detachment volume is determined by the balance of surface tension and buoyancy forces. In other words, the detached bubble volume is not dependent on the gas flow rate, and increasing (or decreasing) the gas flow rate in this regime only increases (or decreases) the frequency of bubble detachment. The dynamic regime happens at intermediate ranges of gas flow rates. In this regime, each bubble can be considered independent of others and inertial, and viscous forces cannot be neglected. At very high flow rates, this regime changes into turbulent regime in which a gas jet is eventually formed [3]. Oguz and Prosperetti [4] proposed a critical flow rate for the upper bound of quasi-static regime. The present study will focus on the quasi-static bubble growth.

During the last decades, a great progress in computational systems and numerical methods has made it possible to numerically study the complex phenomena such as two-phase systems. In two-phase systems, a common approach is to solve one set of Navier–Stokes equations on a stationary grid for the whole flow field which is categorized as one-fluid approach, and the interface is mostly determined by Eulerian interface-capturing or Lagrangian front-tracking methods. In front-tracking methods based on Unverdi and Tryggvason [5], a set of points are tracked on the Lagrangian interface. These points are advected with the flow, and the interface is determined by connecting these points with lines in 2D and with triangular elements in 3D. In interface-capturing method, the interface is identified by a marker function that is advected by the flow. In this method, the interface is captured implicitly contrary to the front-tracking method where the interface is determined explicitly. The marker function can be volume fraction (volume of fluid method) or distance function (level-set method), etc.

These methods have been extensively developed and used in two-phase systems such as bubble formation and rising. The volume of fluid (VOF) method defines a volume fraction α which is 1 for one fluid and 0 for the other one, and the cells including the interface have a value between 0 and 1. α is advected with the flow, and in the case of incompressible flow, this leads to the conservation of volume fraction, and thus the VOF method is mass conservative. The reconstruction of interface can be made by geometrical or compressive schemes. For the case of geometrical schemes, the simplest method (SLIC) was introduced by Noh and Woodward [6]. The simple line interface calculation method approximates the interface as lines parallel to the y-axis for x-direction advection and vice versa. Hirt and Nichols [7] presented a slightly different method in which the interface is approximated by lines, but their orientation is the same for both directions of the advection. Also Youngs [8] introduced a piecewise linear interface calculation (PLIC) method in which the interface is approximated by lines, and the orientations of the lines are normal to the interface. Contrary to the geometrical schemes, in compressive schemes, the convective term in the VOF advection equation is discretized by a compressive differencing scheme which is defined for retaining the sharpness of the interface (CICSAM [9], compressive model in OpenFOAM® [10]). There is no need for any geometrical reconstruction of the interface in algebraic methods, and also their extension to 3D and unstructured meshes is straightforward [11].

Bubble motion and its free rise have received considerable attention and have been extensively investigated using various numerical methods [12–14]. However, the formation of the bubble is more challenging because of the large and fast changes in the surface tension force, particularly when the capillary and Bond numbers are low as in this case the magnitude of surface tension is large in comparison with the buoyancy force [15]. Li et al. [16] performed a numerical study (VOF method) of bubble formation behavior at various pressures, which was an early attempt to investigate the bubble deformation by VOF method. They reported that for a given gas flow rate, the effect of pressure on bubble formation is negligible. Valencia et al. [17] investigated the bubble formation using the VOF method implemented in the commercial solver Fluent. They numerically obtained large bubbles in comparison with the theoretical values, which was attributed to the fact that they took into consideration the adhesion of water and wall in the numerical method. The same method and software were used by Ma et al. [18] to investigate the effect of liquid and orifice parameters on the bubble formation in a 2D domain. The level-set method was introduced by Osher and Sethian [19] and was further developed by Sussman et al. [12] for multiphase flows. This method was also used to study the bubble rise [20] or the contact line in the bubble formation simulation [21], where the effect of wettability was inspected. Sussman and Puckett [22] presented CLSVOF (coupled level-set volume of fluid) method for two-phase flows which is a combination of LS and VOF methods. Buwa et al. [23] used CLSVOF to investigate bubble formation regimes. Albadawi et al. [15] examined the characteristics of bubble growth and detachment at low capillary and Bond

numbers by using four interface-tracking methods, including VOF-Comp. They reported that for the flow rate of 150 mlph, OpenFOAM underestimates the bubble growth and detachment with an error of 37%, which is due to the greater importance of surface tension force relative to the buoyancy force. The VOF function is a discontinuous function over cells, and the computed normal vector of the interface may generate unphysical spurious currents [24]. Therefore, by increasing the accuracy of the computation of normal vectors, the surface tension force is determined more accurately. Georgoulas et al. [25] used a Laplacian filter to smooth the volume fraction function. They reduced the bubble detachment time error to 10% and investigated the effect of gravity levels. Wu et al. [26] numerically investigated the bubble growth and detachment in the presence of cross flow.

Despite numerous works on bubble formation in Newtonian fluids, there are only few numerical studies associated with the non-Newtonian fluids. Ghosh and Ulbrecht [27] studied theoretically and experimentally the bubble formation in shear-thinning and viscoelastic liquids and proposed a model to determine the bubble growth rate and final bubble size. Terasaka and Tsuge [28] investigated the bubble formation at a single orifice in a viscoelastic fluid and presented a model for non-spherical bubble formation. Li [29] and Li et al. [16] also developed a mathematical model for bubble formation at an orifice in non-Newtonian liquids under constant flow rate conditions.

It seems that further research should be done to obtain a better understanding of bubble formation in non-Newtonian liquids. In the present study, bubble formation in non-Newtonian fluids is studied numerically by using a compressive VOF method. In this research, a Laplacian filter is also implemented to study the bubble formation in power-law liquids. At first, the method is explained, and then it is evaluated using experimental results. Afterward, the effects of liquid properties on the bubble formation and detachment are investigated at low capillary and Bond numbers.

2 Numerical formulation

2.1 Governing equations

The governing equations are Navier–Stokes equations which are written in conservative form as follows:

$$\nabla \cdot \vec{U} = 0 \quad (1)$$

$$\frac{\partial}{\partial t} (\rho \vec{U}) + \nabla \cdot (\rho \vec{U} \vec{U}) = -\nabla p + \nabla \cdot \left[\mu (\nabla \vec{U} + \nabla \vec{U}^T) \right] + \rho \vec{g} + \vec{F}_\sigma \quad (2)$$

where \vec{U} , ρ , μ , p and \vec{g} are the fluid velocity, density, viscosity, pressure, and gravitational acceleration, respectively. In addition, \vec{F}_σ is the surface tension force which is applied at the interface of fluids.

2.2 Interface-capturing method

In two-phase systems, the interface must be tracked. One of the interface-capturing methods is volume of fluid (VOF) method. In this method, volume fraction α is 1 for the cells containing only liquid fluid and 0 for the cells containing only gas fluid, and it is between 0 and 1 for the cells including the interface, and the advection equation is solved for the volume fraction. This equation is as follows:

$$\frac{\partial \alpha}{\partial t} + \nabla \cdot (\alpha \vec{U}) = 0 \quad (3)$$

Density (ρ) and viscosity (μ) in the solution domain are determined as the weighted averages over the two phases:

$$\begin{aligned} \rho &= \rho_l \alpha + \rho_g (1 - \alpha) \\ \mu &= \mu_l \alpha + \mu_g (1 - \alpha) \end{aligned} \quad (4)$$

where l and g indicate liquid and gas, respectively.

For shear-thinning time-independent non-Newtonian fluids, several mathematical models have been suggested to characterize their rheological properties. Carreau model [30] is one of the most accurate models which has a good precision at very low and very high shear rates as well as power-law region at intermediate

shear rates. However, in the present study, as the shear rates values are in the intermediate region, the power-law model for its simplicity is used, and the liquid viscosity is calculated by the following power-law model:

$$\mu_l = k(\dot{\gamma})^{n-1} \quad (5)$$

in which; k , $\dot{\gamma}$ and n are consistency (Pa s^n), shear rate (s^{-1}) and flow behavior index (dimensionless), respectively.

In OpenFOAM, a compressive term is added to the volume fraction equation to sharpen the interface:

$$\frac{\partial \alpha}{\partial t} + \nabla \cdot (\alpha \vec{U}) + \nabla \cdot (\alpha (1 - \alpha) \vec{U}_r) = 0 \quad (6)$$

where $\vec{U}_r = \vec{U}_l - \vec{U}_g$ is the compressive velocity which is taken into consideration only in the interface region due to the term $(\alpha (1 - \alpha))$ [31]. \vec{U}_r (relative velocity at the faces of the cells) is calculated based on the magnitude of maximum velocity in the interface region, and its direction is the normal vector of the interface as follows:

$$\vec{U}_r = \vec{n}_f \min \left(C_\alpha \frac{|\phi|}{|S_f|}, \max \left(\frac{|\phi|}{|S_f|} \right) \right) \quad (7)$$

where \vec{n}_f , ϕ , and S_f are the unit normal vector of the cell face, mass flux, and the cell surface area, respectively. Furthermore, the value of C_α is 1 in the present study. If C_α is set to zero, the compressive term vanishes, and Eq. (6) simplifies to Eq. (3).

VOF uses CSF model of Brackbill et al. [32] to calculate the surface tension force as follows:

$$\begin{aligned} \vec{F}_\sigma &= \sigma \kappa \nabla \alpha \\ \kappa &= \nabla \cdot \left(\frac{\nabla \alpha}{|\nabla \alpha|} \right) \end{aligned} \quad (8)$$

where σ and κ are surface tension and curvature, respectively.

2.2.1 VOF smoothing

As mentioned, the VOF function is a discontinuous function over cells and the computed normal vector of the interface which is used in the calculation of the surface tension force may generate unphysical spurious currents [24]. In this study, similar to the approach adopted by Hoang et al. [33] and Georgoulas et al. [25], the spurious currents are suppressed by revising the calculation procedure of interface curvature in OpenFOAM solver (interFoam). In this way, the volume fraction is smoothed with a Laplacian filter before the calculation of curvature as follows:

$$\begin{aligned} \tilde{\alpha}_p &= \frac{\sum \alpha_f S_f}{\sum S_f} \\ \kappa &= \nabla \cdot \left(\frac{\nabla \tilde{\alpha}}{|\nabla \tilde{\alpha}|} \right) \end{aligned} \quad (9)$$

in which subscripts f and p indicate the face and cell index, respectively, and α_f is the value of α at the face center which is linearly interpolated. The filter can be repeated more than once to achieve suitable smoothed field. For the present paper, initial trial simulations showed that the five times smoothing is adequate. It should be noted that the smoothed volume fraction is only used in the calculation of curvature, and in other parameters, such as density and viscosity, the volume fraction is non-smoothed.

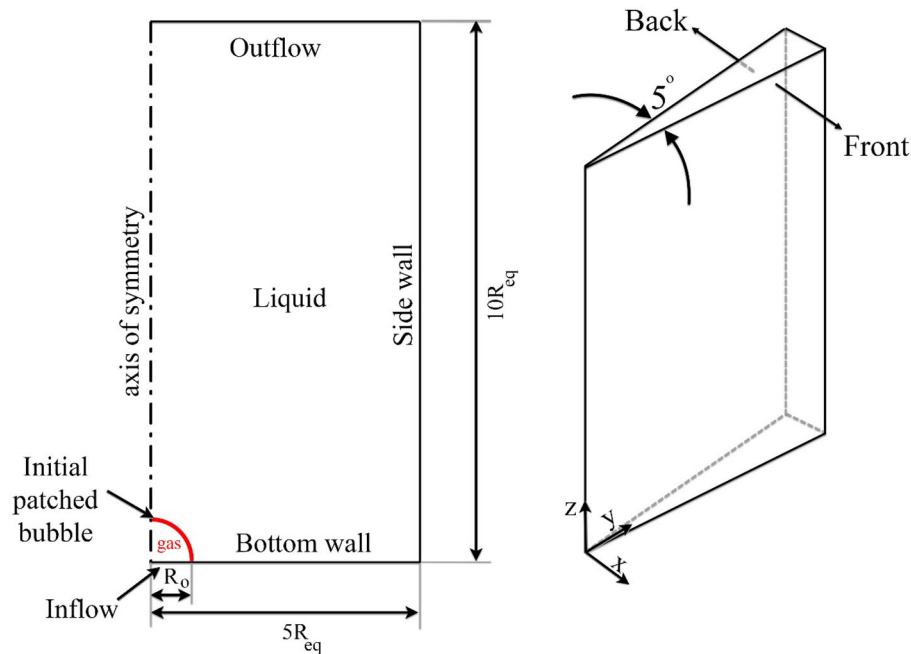


Fig. 1 Schematic of computational domain and boundary conditions

2.3 Simulation parameters

As mentioned before, the numerical simulation is done by using OpenFOAM (ver. 2.3.1) and by improving (smoothing) the solver “interFoam”. The PISO (pressure implicit with splitting of operators) algorithm is used for pressure–velocity coupling. In the equations, the $\partial/\partial t$ terms are discretized by CrankNicolson 1 scheme. The time step is adaptively determined by the maximum Courant number which is set to 0.1; accordingly, the time step is about 10^{-6} s in the present study. In compressive schemes, the maximum Courant number is important [34], and in this research, it is determined by initial trial simulations; the difference between the detachment times for the Courant numbers of 0.1 and 0.01 is less than 2% ; so the value of 0.1 is selected for the maximum Courant number. In Equation (2), the convection and Laplacian terms are discretized using Gauss limited LinearV 1.0 and Gauss linear corrected schemes, respectively, but in Eq. (6), the convection term $\nabla \cdot (\alpha \vec{U})$ is discretized by Gauss vanLeer scheme [35] which has a limiter to preserve the volume fraction in the range of [0, 1], and the compressive term $(\nabla \cdot (\alpha(1 - \alpha)\vec{U}_r))$ is discretized using the Gauss interface compression scheme described by Rusche [36] to provide smoother interface and confirm the boundedness of the volume fraction field.

2.4 Computation setup

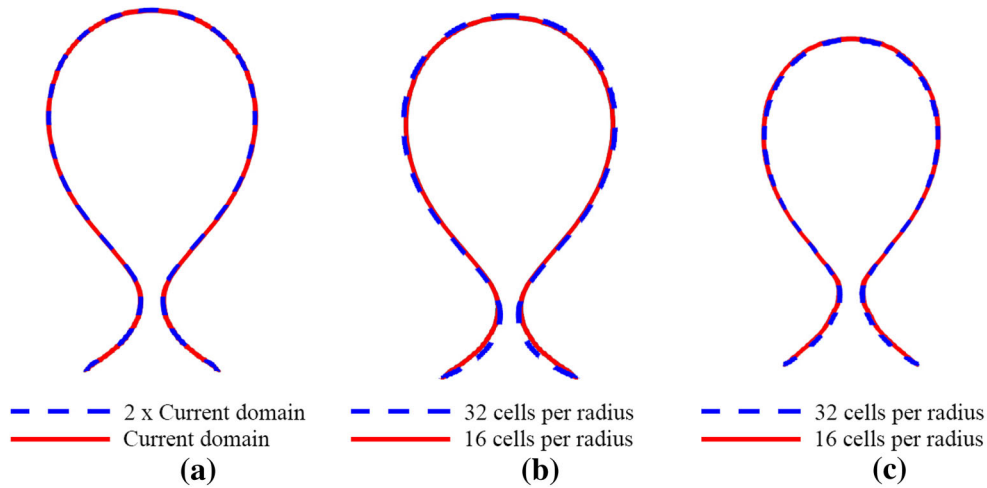
Since the bubble formation at an orifice in a stagnant liquid can be assumed to be axisymmetric, in the present study, an axisymmetric computational domain is considered. A 5-degree section of the 3D physical domain (wedge shape) is considered as the computational domain. The schematic of computational domain and boundary conditions are illustrated in Fig. 1.

To avoid any effect from the boundaries, the general domain size is assumed to be $10 \times 20 \text{ mm} \sim 5R_{eq} \times 10R_{eq}$, where R_{eq} is the bubble detachment equivalent radius [15]. Mesh dependency studies showed that with 16 computational cells per orifice radius, the numerical solution can be considered mesh-independent; this result is also in agreement with the earlier similar studies [15,25]. The quantitative investigation on domain and mesh size for a sample case is given in Table 1 and Fig. 2, respectively. The relative errors are under 4%, and the bubble profiles are almost the same so that the mentioned sizes are chosen for further simulations.

The front and back faces have wedge boundary condition. At the inlet, the flow is supposed to be fully developed and the inflow velocity profile is parabolic. The magnitude of the axial velocity is $u =$

Table 1 Domain and mesh independency for the case $Bo = 0.5$, $Ca = 10^{-1}$

Case	Cells per orifice radius	Detachment time (s)	Detachment volumes (μm^3)	Time relative error (%)	Volume relative error (%)
Current domain ($n = 1$)	16	0.190	9.00	0	0
$2 \times$ current domain ($n = 1$)	16	0.190	9.00		
Newtonian ($n = 1$)	16	0.190	9.00	4.0	3.6
Newtonian ($n = 1$)	32	0.198	9.32		
Non-Newtonian ($n = 0.2$)	16	0.119	6.06	1.7	1.8
Non-Newtonian ($n = 0.2$)	32	0.117	5.95		

**Fig. 2** Bubble profiles at detachment time for the case $Bo = 0.5$, $Ca = 10^{-1}$: **a** current domain (red solid line) and double of the current domain (blue dash line), **b** Newtonian ($n = 1$) with 16 cells per radius (red solid line) versus 32 cells per radius (blue dash line), **c** non-Newtonian ($n = 0.2$) with 16 cells per radius (red solid line) versus 32 cells per radius (blue dash line) (color figure online)

$u_{\max} (1 - (x/R_0)^2)$ in which $x = 0$ is the axis of symmetry where the velocity is maximum and $x = R_0$ is orifice radius where the velocity turns into zero. The value of maximum velocity is determined by the flow rate Q and it is equal to $u_{\max} = 2Q / (\pi R_0^2)$. For the pressure, fixed-flux pressure boundary condition is used to adjust the pressure gradient in a way that the flux on the boundary is equal to that determined by the velocity boundary condition. For volume fraction, a constant boundary condition is applied. At the outlet, the outflow condition is used and the pressure is adjusted to atmospheric pressure; also, for the volume fraction, the zero gradient boundary condition is imposed. At the walls, the no-slip and zero gradient boundary conditions are applied for the velocity and pressure, respectively. At the bottom wall, for volume fraction, the static contact angle is set to $\theta_s = 20^\circ$ [15]. To model the wall adhesion, Brackbill et al. [32] defined the normal to the interface at the wall (\vec{n}) as follows:

$$\vec{n} = \vec{n}_{\text{wall}} \cos \theta_s + \vec{n}_t \sin \theta_s, \quad (10)$$

where θ_s , \vec{n}_{wall} and \vec{n}_t are the static contact angle, the unit normal vector directed to the wall pointing to the wall, and the unit vector tangential to the wall pointing toward the liquid, respectively. From a numerical point of view, Gerlach et al. [37] reported that the imposed static contact angle influences the bubble formation process; however, below a critical value of the contact angle, bubble is pinned to the orifice rim, and therefore, the contact angle does not affect the volume of the detached bubble. The value of 20° is selected for the static contact angle in order to keep the bubble at the orifice, as experimentally observed by Albadawi et al. [15].

3 Numerical method validation

Before investigating the bubble formation in shear-thinning liquids, at first the numerical simulation is validated with the previous studies. It should be mentioned that although the validation problem is examined in a

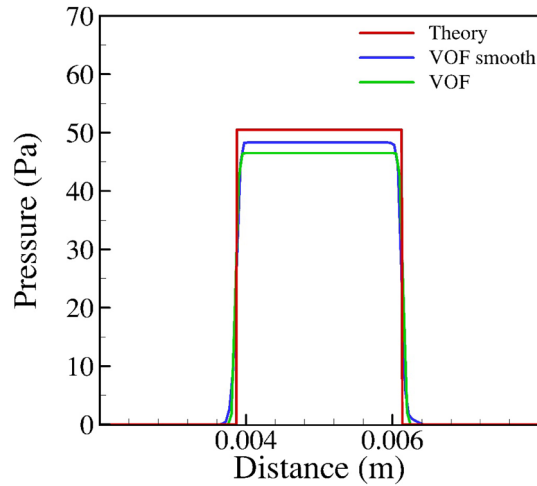


Fig. 3 Numerical and theoretical results for Laplace pressure difference (Brackbill's test case)

Newtonian fluid, the method can be used for non-Newtonian liquids as well, because the interface-capturing method (VOF-smooth) works independently of viscosity.

At first, in order to validate the solver for the bubble problem, the widely used Brackbill's test case [38] is applied. In this test case, initially, a cuboidal bubble is set in the middle of a stationary liquid domain which has different viscosity and density, and it is let to reach its equilibrium state while zero gravity is applied. At the final state, a bubble with spherical shape with a pressure difference with the surrounding liquid (Laplace pressure) should be in the center of the computational domain. The numerical results and theoretical value obtained from the Laplace equation are presented in following figure. Figure 3 shows that the improved solver has a better prediction of the theoretical pressure difference and the relative pressure difference obtained from VOF (OpenFOAM), VOF-smooth with theoretical value are 10% and 5% respectively.

3.1 Problem definition

With the purpose of verifying the numerical model, the recent study of Albadawi et al. [15] and Georgoulas et al. [25] was selected which has adequate information to reproduce it numerically. The problem is the formation of air bubbles at an orifice in a quiescent water. The air is injected at a constant flow rate Q which is small enough so that the bubble formation regime is quasi-static. Albadawi et al. [15] investigated the problem experimentally and numerically using interFoam solver, and Georgoulas et al. [25] used interFoam solver with filter.

The experimental facility of Albadawi et al. [15] involved a stainless steel surface with an orifice of 1.6 mm diameter which was put to a depth of 20 mm under the water surface in a glass tank with a cross-sectional area of 50×50 mm. A combination of a Hamilton (Gastight 1002 series) 2.5-ml syringe and a kdScientific (KDS 200 cz) infusion pump controlled the rate of gas flow. To capture images, a single NAC Hi-Dcam II high-speed (frame rate of 1000 Hz) digital video camera was used with an exposure time of 0.5 ms to have sharp images. The bubble was illuminated with a diffused backlight containing six 300-lm LED bulbs. The tank was filled with ultra-pure water which was purified with a Millipore purification system. To detect the boundary of the bubble, an image processing code was developed, which according to the authors, the uncertainty in detecting the boundary of the bubble was ± 1 pixel, which corresponded to a value of ± 0.0134 mm. More information about the validation case has been presented in the study of Albadawi et al. [15]. The liquid/gas properties and other parameters are given in Table 2. The orifice radius is 0.8 mm, and as mentioned before, 16 computational cells per orifice radius are needed; therefore, the uniform grid size is 200×400 cells.

3.2 Validation results

In Fig. 4, the numerical and experimental results are compared. Albadawi et al. [15] reported the bubble shape at six different frames $t^* = t/t_{\text{det}} \sim 0, 0.2, 0.4, 0.6, 0.8, 1$. It should be noted that at $t^* = 0$, a hemisphere

Table 2 Physical properties of fluids in validation case [15]

Parameters	Symbols	Values	Units
Liquid density	ρ_l	998.2	kg/m ³
Liquid viscosity	μ_l	0.001	kg/ (m s)
Gas density	ρ_g	1.225	kg/m ³
Gas viscosity	μ_g	1.79×10^{-5}	kg/ (m s)
Gravity	g	9.81	m/s ²
Orifice radius	R_o	0.8	mm
Flow rate	Q	150	mlph
Surface tension	σ	0.073	N/m

bubble was patched numerically in the present work as well as Albadawi et al. [15]. As can be seen from Fig. 4, the present numerical results are in excellent agreement with the experimental data even at detachment time. The detachment time and the volume of the bubble at the moment of detachment are tabulated and compared with that in the previous studies in Table 3. t_{det} , CG, and V_{det} stand for time of detachment, center of gravity, and volume of detachment, respectively. The errors (Et_{det} and EV_{det}) are relative errors; for instance, Et_{det} is computed as $Et_{det} = (t_{num} - t_{exp})/t_{exp} \times 100$ where num and exp indicate numerical and experimental values, respectively. As it is observed in Table 3, by smoothing, the relative error decreases from 37 to 9.8% in Georgoulas et al. [25] and to 6.7% in the present work. The reason is that by smoothing, the surface tension force is computed more accurately. There are two differences between the Georgoulas et al. [25] study and the present research that cause this study to have a lower error. First, the number of smoothing was 5 in the present study, and it was 2 in Georgoulas et al. [25]. Furthermore, as mentioned before, the maximum Courant number is an important parameter in a compressive scheme, and its value was 0.1 in this research. However, it was 0.2 in Georgoulas et al. [25] work. Consequently, the relative errors are adequately low for the purpose of studying bubble formation characteristics.

4 Results and discussion

In this section, the process of bubble formation in non-Newtonian shear-thinning liquids is investigated. At first, the overall process and then the formation parameters are studied.

4.1 Non-Newtonian bubble formation

In this part, the shear-thinning effect is examined. To have more universal results, the results are shown by non-dimensional numbers such as Bond number, $Bo = \frac{\rho_l g R_o^2}{\sigma}$, and capillary number, $Ca = \frac{\mu_l v_g}{\sigma}$, where ρ_l , μ_l , R_o , v_g and \vec{g} are liquid density, liquid viscosity, orifice radius, gas velocity magnitude, and gravitational acceleration, respectively. Bo number demonstrates the ratio of buoyancy force to surface tension force and Ca number shows the ratio of viscous force to surface tension force.

As discussed earlier, in this research, the focus is on low Bond and capillary numbers. Therefore, these numbers were investigated in the present study: $Bo = 0.05, 0.1, 0.5$ and $Ca = 10^{-1}, 10^{-2}, 10^{-3}, 10^{-4}$. The parameters were set as follows: $g = 9.8 \frac{m}{s^2}$, $R_o = 0.8$ mm, $Q = 150$ mlph and $\sigma = 0.028 \frac{N}{m}$. Also, the viscosity and density were chosen so that the Bond and capillary numbers matched the mentioned values ($226 \leq \rho \leq 2261 \frac{kg}{m^3}$ and $1.37 \times 10^{-4} \leq \mu \leq 1.37 \times 10^{-1} \text{kg/ (m s)}$). The orifice radius effect is considered in many studies (such as [39–41]) and in the current study is kept constant.

For instance, Fig. 5 displays the bubble formation sequences for the case $Bo = 0.5$, $Ca = 10^{-2}$, $n = 0.2$ at various moments, including initial state, expansion, necking, and detachment.

Figure 6 shows the center of gravity of the bubble during its formation for $Bo = 0.5$ and various Ca numbers. As it is observed, for some Ca numbers, there is no difference between the results of the Newtonian and non-Newtonian liquids (Fig. 6a, b). However, in some cases (Fig. 6c, d), they are different. For Newtonian liquids, the detachment time and consequently the detachment volume generally increase with increasing the capillary number. As mentioned above, by increasing the capillary number, or in other words, by increasing the viscosity, the magnitude of the resistance force rises. Consequently, the buoyancy force must be greater

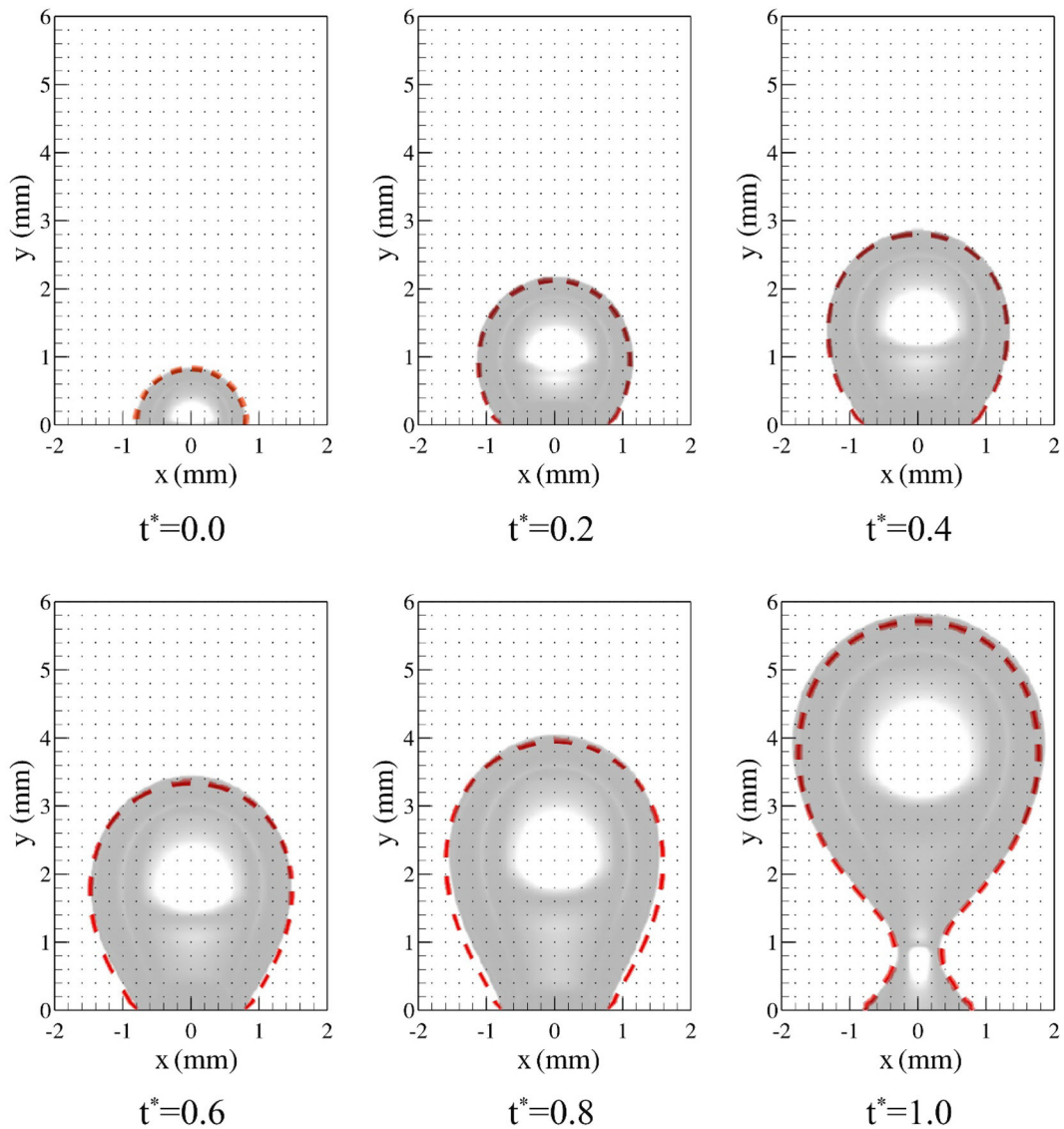


Fig. 4 Comparison of the present numerical simulation results and experimental data of Albadawi et al. [15]. The background bubble is the experimental bubble shape and the dashed line indicates our numerical simulation

Table 3 Comparison of bubble detachment volumes and bubble detachment times obtained from the experimental and numerical results

Method	Reference	t_{det} (s)	Et_{det} (%)	CG (mm)	ECG (%)	V_{det} (mm ³)	EV_{det} (%)
Experimental results	Albadawi et al. [15]	0.684	0	3.625	0	29.699	0
VOF (ANSYS Fluent)	Albadawi et al. [15]	0.834	21.9	3.917	8.05	35.804	20.56
VOF (OpenFOAM) original	Albadawi et al. [15]	0.429	-37.2	3.209	-11.47	21.022	-29.22
VOF (OpenFOAM) smooth	Georgoulas et al. [25]	0.617	-9.8	Not reported	Not reported	26.769	-10.9
VOF (OpenFOAM) smooth	Present work	0.638	-6.7	3.49	-3.72	27.934	-5.9

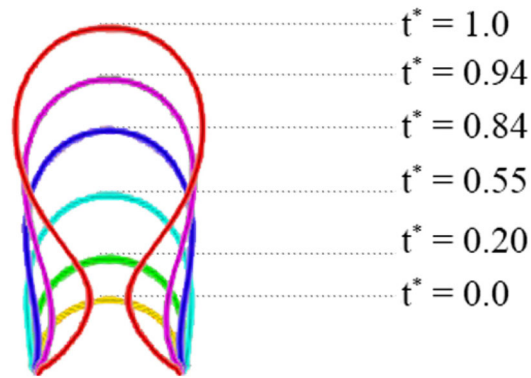


Fig. 5 Bubble formation sequences for the case $Bo = 0.5$, $Ca = 10^{-2}$, $n = 0.2$, $t^* = t/t_{det}$. In this case, $t_{det} = 119$ ms

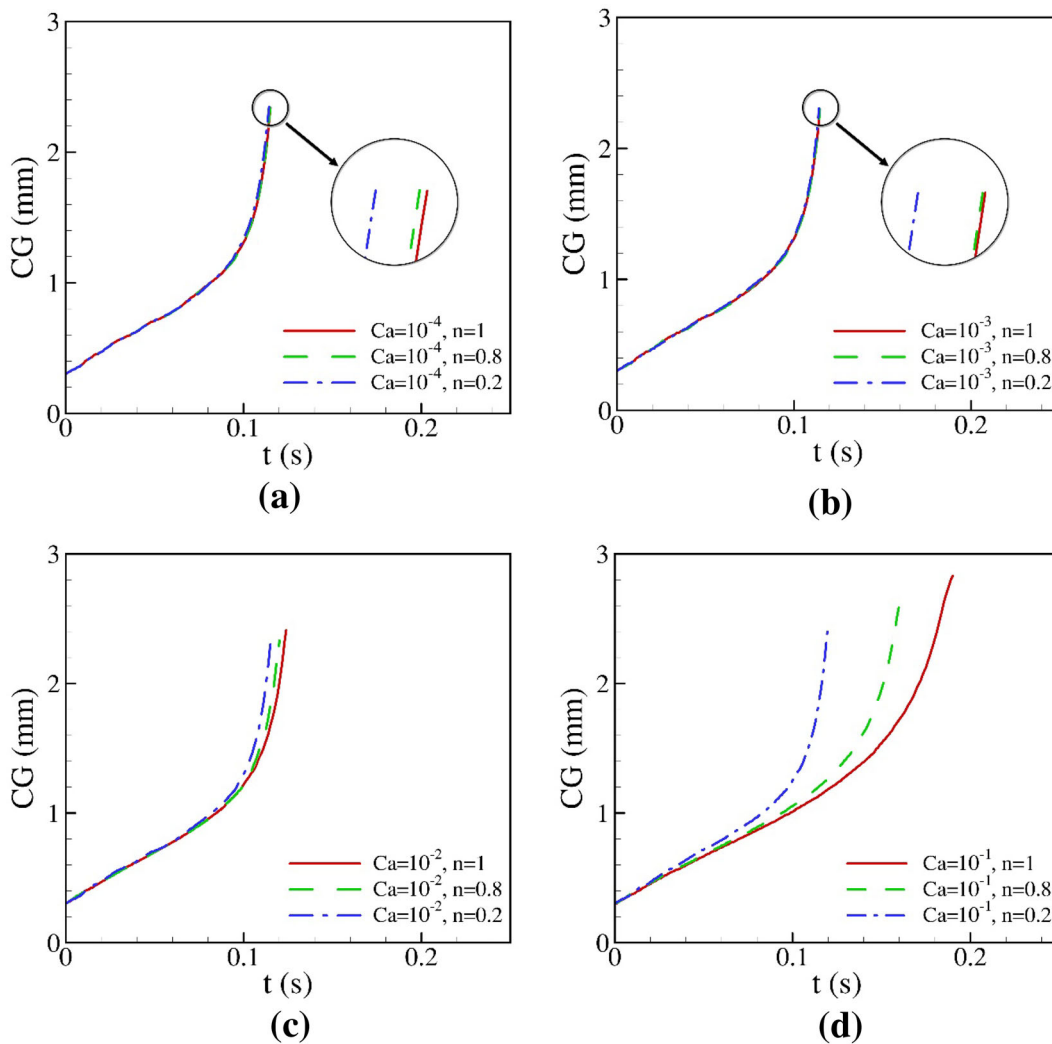


Fig. 6 Center of gravity of the bubble until the detachment point for $Bo = 0.5$. **a** $Ca = 10^{-4}$, **b** $Ca = 10^{-3}$, **c** $Ca = 10^{-2}$ and **d** $Ca = 10^{-1}$

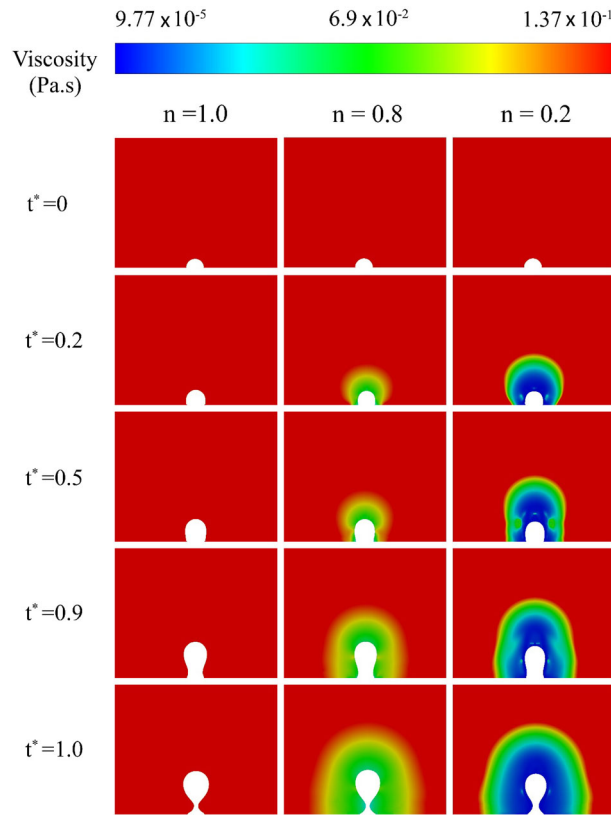


Fig. 7 The viscosity contours for case $Bo = 0.5$ and $Ca = 10^{-1}$ and for Newtonian ($n = 1$) and non-Newtonian ($n = 0.8$ and $n = 0.2$) liquids at frames: $t^* = t/t_{det} = 0, 0.2, 0.5, 0.9$ and 1.0

in order to detach the bubble from the orifice and as a result, the bubble detachment volume increases. When the Newtonian liquid is changed to a shear-thinning non-Newtonian fluid, the viscosity around the bubble decreases locally due to the shear rate, which results in lower resistance force and lower detachment volume. This phenomenon is better understood from Fig. 6d, in which the bubble detachment time and volume are reduced by increasing the shear-thinning effect (i.e., by decreasing n). The local viscosity in this case is shown in Fig. 7. In the Newtonian case ($n = 1$), the viscosity is constant during the bubble formation. When the liquid is shear-thinning ($n = 0.8$ or $n = 0.2$), at $t^* = 0$, because of no shear rate the viscosity is constant and the same as the Newtonian one. After that, due to the presence of shear rate around the bubble, the local viscosity decreases and this reduction is higher for $n = 0.2$ than for $n = 0.8$ as expected. One of the regions of high shear rate is on the top of the bubble tip, as can be seen in Fig. 7. The reason is that as the bubble expansion occurs, the liquid is pushed up by the tip of the bubble. In addition, in the necking stage, the neck region experiences large variations just before the detachment which means high shear rate and low viscosity; this can be seen at $t^* = 1.0$ for $n = 0.8$ or 0.2 .

In Fig. 8, the ratio of bubble detachment volume for $n = 0.2$ to that for $n = 1.0$ (i.e., the ratio of detachment volume for shear-thinning non-Newtonian fluid to that for Newtonian fluid) is shown. For non-Newtonian fluid, if the apparent viscosity falls below a limiting value, it practically loses its effect on bubble formation, and the buoyancy force balances only with the surface tension force. In these cases, there is no difference between the results of Newtonian and non-Newtonian liquids. Thus, bubble detachment volumes and times are like each other.

According to the results, it seems that for a given Bond number, there is a critical capillary number below which there is no difference between the detachment volumes. In addition, for non-Newtonian fluid, if apparent capillary number obtained by apparent viscosity is lower than the critical capillary number, the detachment volume is the same as the corresponding Newtonian case. By initial trial simulations, the critical capillary numbers for $Bo = 0.5, 0.1$ and 0.05 were found to be about 1.5×10^{-3} , 1.5×10^{-2} and 1.0×10^{-2} respectively. For this matter, in Fig. 6a, b, the capillary number is less than 1.5×10^{-3} and consequently, the plots coincide with each other.

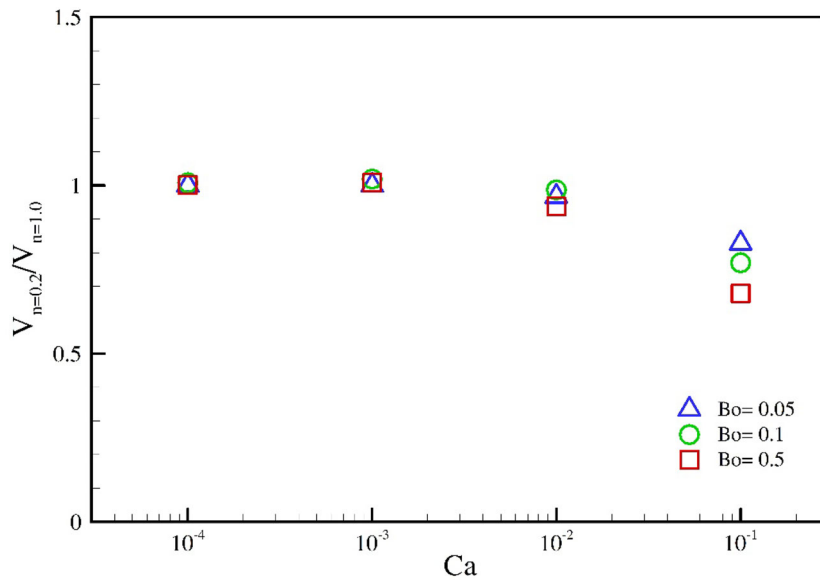


Fig. 8 Ratio of bubble detachment volume for $n = 0.2$ to that for $n = 1.0$

4.2 Bubble velocity

The velocity of the bubble during its formation can be obtained by differentiating the position graph. For instance, for the case $Bo = 0.5$ and $Ca = 10^{-1}$, the velocity is presented in Fig. 9a. The bubble velocity gradually increases and accelerates before the detachment. As the shear-thinning effect increases, the viscosity decreases, and therefore, the drag force is reduced. As a result, the velocity at the moment of detachment increases and the bubble starts to rise with a higher velocity. If velocity is plotted as a function of $t^* = t/t_{det}$ (Fig. 9b), it can be interestingly seen that the velocities are almost the same up to 70% of the formation process. This point (which can be interestingly seen later in Fig. 11b) is the start of elongation and necking stages, which means that the shear-thinning effect does not affect the bubble velocity in the expansion stage.

4.3 Contact angle

The instantaneous contact angle (the angle between the wall and bubble interface as illustrated in Fig. 10) varies during the process of bubble formation. In the first stage of growth, as the shape of the bubble changes from hemispherical to truncated spherical shape, the angle decreases over time, and it remains nearly constant until the start of necking. Afterward, the bubble is elongated along the vertical direction, and consequently, the instantaneous contact angle grows gradually with time. Just before the detachment, the angle increases rapidly and the bubble detachment occurs. The same behavior has been described by Di Bari et al. [42] and Albadawi et al. [15].

In Fig. 11a, instantaneous contact angle for Newtonian ($n = 1.0$), low shear thinning ($n = 0.8$) and high shear thinning ($n = 0.2$) fluids is shown as a function of time for $Bo = 0.5$ and $Ca = 10^{-1}$. As mentioned before, by increasing the shear-thinning effect, the detachment time decreases. However, for all liquids, the graphs in the figure follow the same trend which was previously discussed. This can be better seen in Fig. 11b, in which the contact angle is presented as a function of non-dimensional time. In the region in which the contact angle is nearly constant and the bubble shape is spherical, the contact angle for the Newtonian fluid has the least value; this can be justified as follows: when the shear-thinning effect decreases, the local viscosity rises, and as a result, the viscous force increases and pushes the bubble down, and consequently, the instantaneous contact angle is reduced.

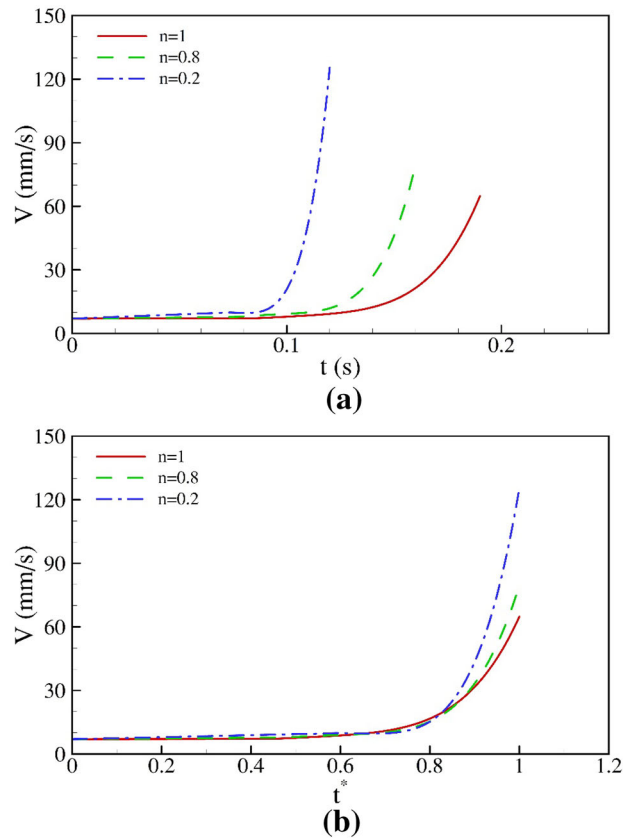


Fig. 9 **a** The velocity of the bubble during its formation for the case $Bo = 0.5$, $Ca = 10^{-1}$, **b** the velocity plots when time is non-dimensionalized by the detachment time: $t^* = t/t_{det}$

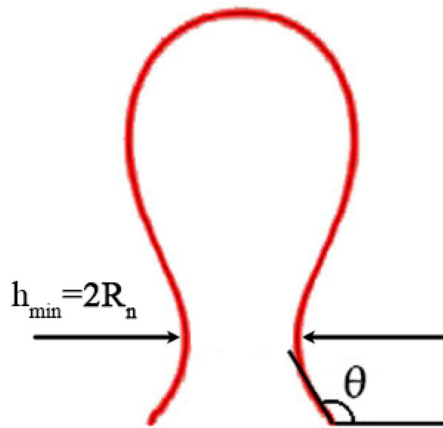


Fig. 10 Illustration of instantaneous contact angle and neck radius

4.4 Detachment process

In the expansion stage, the bubble grows spherically and the buoyancy force increases. When the bubble volume is reached near the detachment volume, the buoyancy becomes comparable to the bounded surface tension force and the collapse stage (necking stage) occurs. Until the start of necking stage, the minimum bubble radius is equal to the orifice radius and in the necking stage, the minimum bubble radius which is also called “necking radius” (R_n) decreases. In this stage, the gas velocity increases under constant flow conditions and the pressure decreases as a result of the Bernoulli effect. The pressure difference between the inside and outside of the

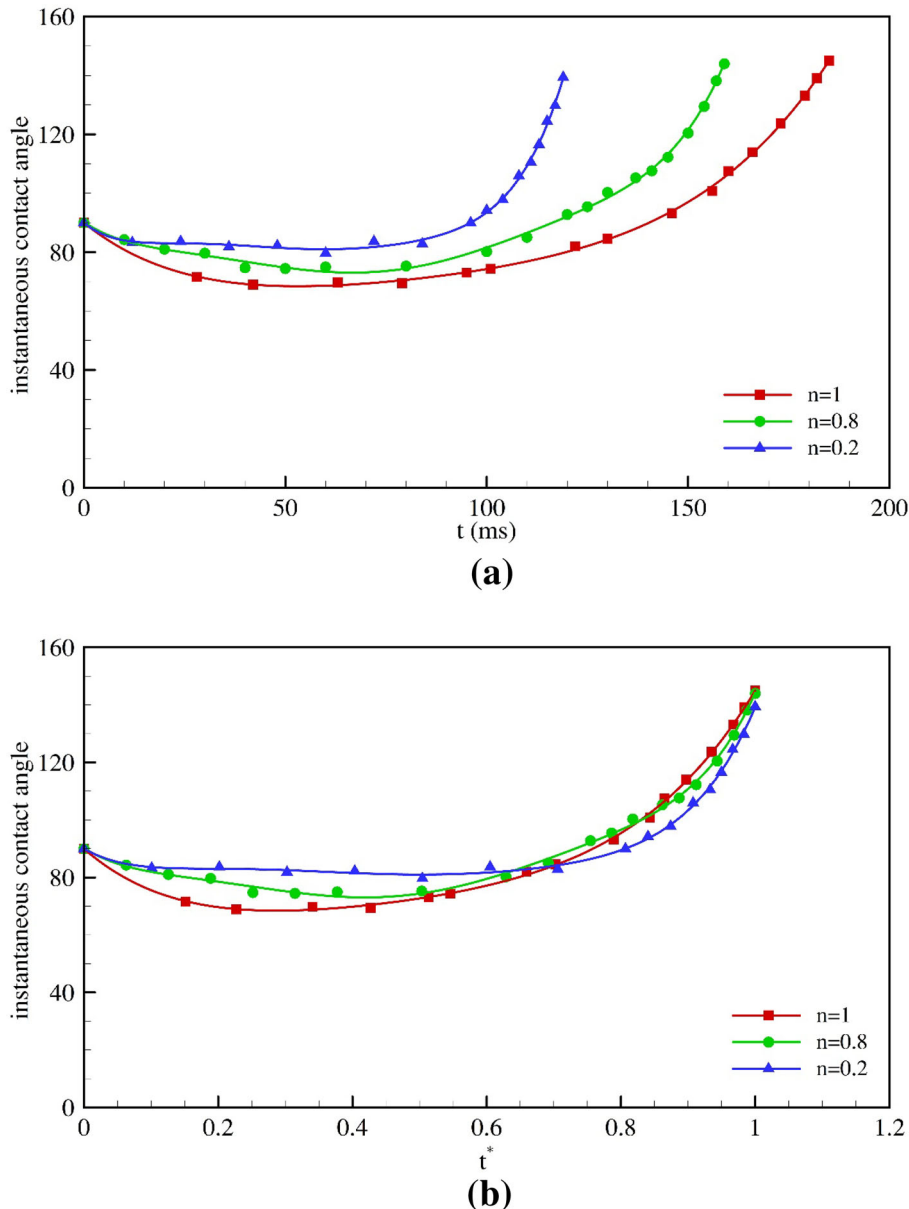


Fig. 11 **a** instantaneous contact angle versus time for the case $Bo = 0.5$ and $Ca = 10^{-1}$, **b** instantaneous contact angle versus non-dimensional time ($t^* = t/t_{det}$) for the case $Bo = 0.5$ and $Ca = 10^{-1}$

neck accelerates the bubble neck pinching. In the literature [43,44], it has been confirmed that a power-law $R_n \propto \tau^\eta$ can be used to characterize the rate of reduction of neck radius just before detachment, where τ is the time until detachment ($\tau = t_{det} - t$). Using experimental observations, Thoroddsen et al. [43] found that η is about 0.57 for air/water systems. Moreover, based on potential flow numerical simulations, Gordillo et al. [44] reported that the exponent varies from 1/2 to 1/3 and is equal to 1/3 when the gas inertia has a large value. Albadawi et al. [11] reported the value of 0.36 using numerical simulation with VOF method. The present value (Fig. 12a) for the air/water case ($\eta = 0.34$) is consistent with previous results especially with the results of Albadawi et al. [11]. In Fig. 12b, for $Bo = 0.5$ and $Ca = 10^{-1}$, the non-dimensional ratio of neck radius to orifice radius is presented for Newtonian ($n = 1.0$), low shear-thinning ($n = 0.8$), and high shear-thinning ($n = 0.2$) liquids. Burton et al. [45] reported that when the viscosity is in the range $10 \text{ cP} < \mu < 100 \text{ cP}$, the exponent varies between 1/2 and 1. For the case $n=1$, the viscosity is 137 cP and the exponent is 0.99, which is in good agreement with the results of Burton et al. [45]. By increasing the shear-thinning effect, the local

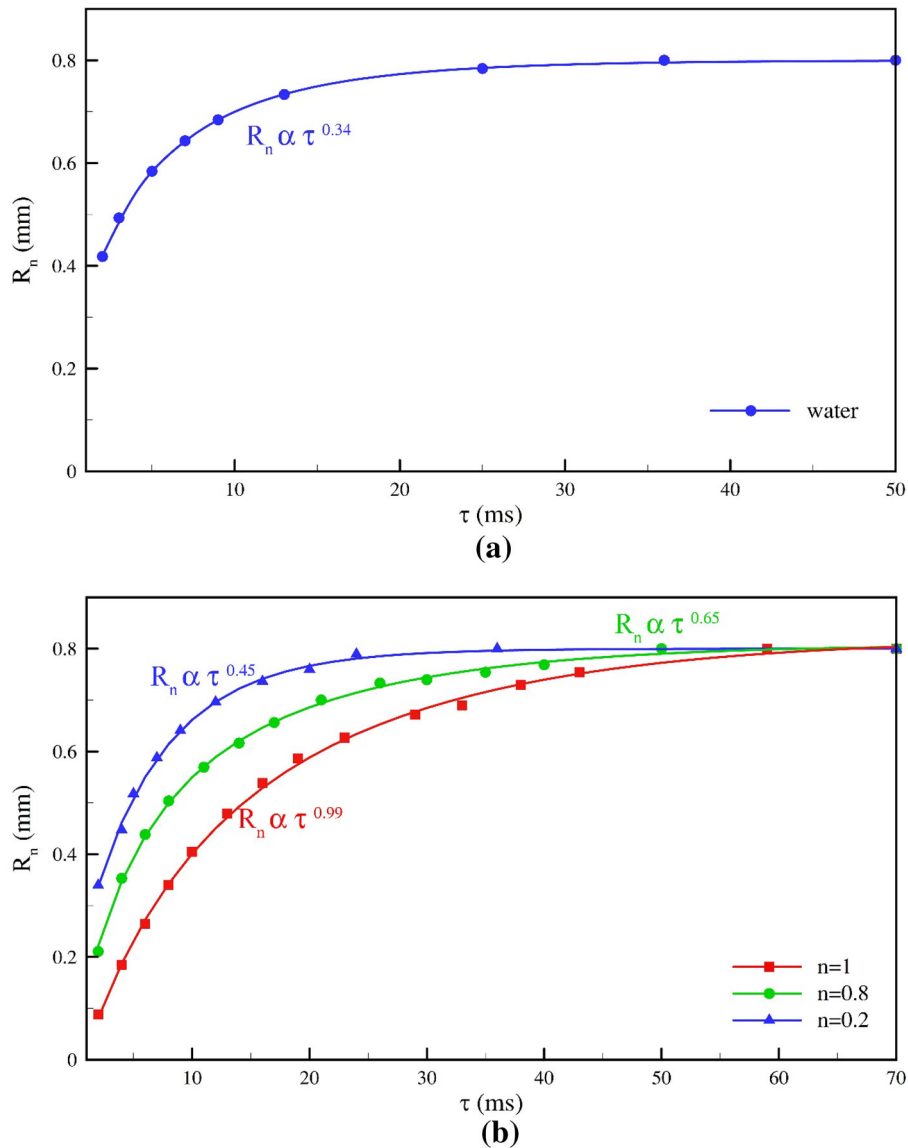


Fig. 12 **a** Non-dimensional ratio of neck radius to orifice radius as a function of time until detachment for water, **b** non-dimensional ratio of neck radius to orifice radius as a function of time until detachment for $Bo = 0.5$ and $Ca = 10^{-1}$

viscosity decreases and the exponent (η) is also reduced. It is good to note that in Fig. 6, the formation process for $Bo = 0.5$, $Ca = 10^{-1}$ and $n = 0.2$ nearly matches that for $Bo = 0.5$, $Ca = 10^{-3}$ and $n = 1.0$ and the viscosity in the latter case has the same order of magnitude as the water viscosity. Consequently, the exponent ($\eta = 0.45$) is consistent with the literature.

4.5 Bubble rise

The bubble continues its ascension after the detachment, as a result of buoyancy force. In Fig. 13, the bubble motion for a sample case is shown for Newtonian and non-Newtonian liquid. In Fig. 13a, b the bubble deforms into an ellipsoidal shape just after detachment and its shape remains constant. So, it is expected that the bubble reaches to its terminal velocity. By increasing the shear-thinning effect and decreasing the liquid viscosity around the bubble, the bubble enters the wobbling region and its shape has fluctuations.

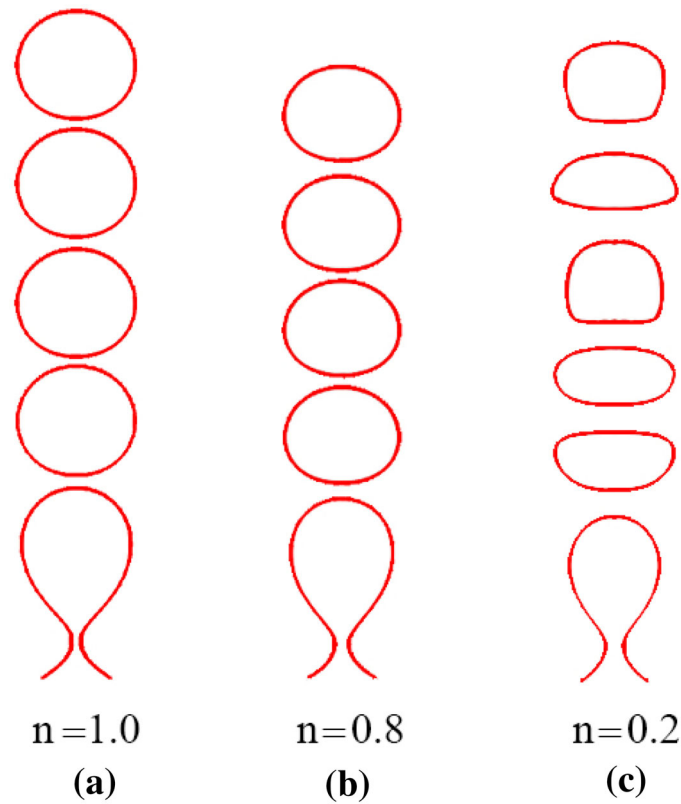


Fig. 13 Bubble motion after the detachment for the case $Bo = 0.5$, $Ca = 10^{-1}$: **a** Newtonian ($n = 1$), **b** non-Newtonian ($n = 0.8$), **c** non-Newtonian ($n = 0.2$)

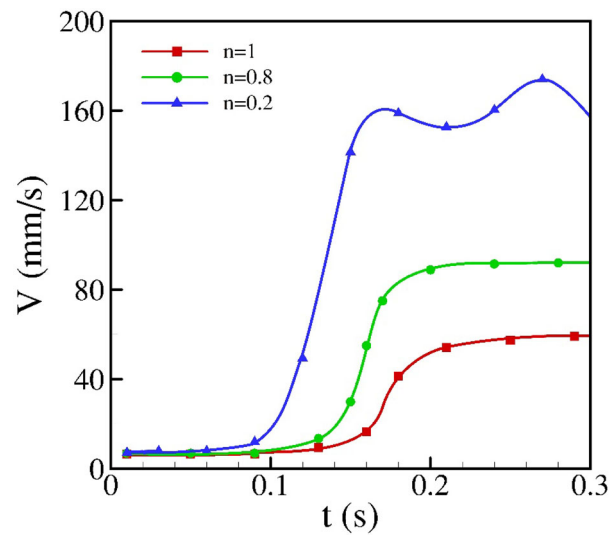


Fig. 14 Bubble center of gravity velocity for the case $Bo = 0.5$, $Ca = 10^{-1}$

In Fig. 14 the bubble (center of gravity) velocity is presented. As expected, by decreasing the power-law index (n) and decreasing the liquid viscosity around the bubble, the velocity of the bubble increases. The terminal velocity for the Newtonian case is 59.5 mm/s which has about 3.5% error with the velocity (57.5 mm/s) obtained from Bhaga and Weber [46] map which is reasonable.

5 Conclusion

In the present study, the bubble formation and detachment in a stagnant shear-thinning liquid were investigated numerically at low capillary and Bond numbers. The VOF solver of OpenFOAM[®] (v. 2.3.1) was improved and used to examine the characteristics of bubble formation. The results obtained from the enhanced model were validated quantitatively which were in excellent agreement with the experimental results in the literature. In addition, the bubble formation in Newtonian and non-Newtonian power-law liquids was modeled to investigate the detachment volume and time as well as other parameters such as instantaneous contact angle and necking radius.

For Newtonian liquids, by increasing the capillary number, the detachment time and consequently the detachment volume generally increased due to the presence of large viscous force. For shear-thinning non-Newtonian liquids, the bubble detachment volume and time were reduced with increasing the shear-thinning effect (i.e., by decreasing “ n ”). However, it was observed that for Newtonian fluids, there is a critical capillary number for a given Bond number below which there is no change in the volume of detachment. Similarly, the results indicated that in non-Newtonian fluids, if apparent capillary number obtained by apparent viscosity is less than critical capillary number, the detachment volume is the same as the corresponding Newtonian case.

For non-Newtonian fluids, by increasing the shear-thinning effect, the bubble was detached with a higher velocity. However, during bubble formation, the shear-thinning effect did not influence the velocity in the expansion stage.

In the bubble formation process, the instantaneous contact angle first decreased and then remained nearly constant and afterward, it increased until the bubble detachment. For shear-thinning liquids, the trend of the contact angle was the same as that for the Newtonian liquids. Furthermore, the maximum values of contact angle were the same as each other. However, in the region in which the contact angle was nearly constant, by decreasing the shear-thinning effect (i.e., by increasing “ n ”), the minimum value of contact angle increased. The reason was that the local viscosity increased and accordingly, the viscous force increased. As a result, the bubble was pushed down and the contact angle decreased.

The variation of neck radius with relative time was modeled using a power relation ($R_n \propto \tau^n$), where the exponent (n) depended on the viscosity. For shear-thinning liquid, by decreasing the flow behavior index (n), the local viscosity around the bubble decreased and consequently, the exponent (n) was reduced.

References

1. Esfidani, M.T., Oshaghi, M.R., Afshin, H., Firoozabadi, B.: Modeling and experimental investigation of bubble formation in shear-thinning liquids. *J. Fluids Eng.* **139**, 071302 (2017)
2. Mählmann, S., Papageorgiou, D.T.: Buoyancy-driven motion of a two-dimensional bubble or drop through a viscous liquid in the presence of a vertical electric field. *Theoret. Comput. Fluid Dyn.* **23**, 375 (2009)
3. Chakraborty, I., Ray, B., Biswas, G., Durst, F., Sharma, A., Ghoshdastidar, P.: Computational investigation on bubble detachment from submerged orifice in quiescent liquid under normal and reduced gravity. *Phys. Fluids (1994-present)* **21**, 062103 (2009)
4. Oguz, H.N., Prosperetti, A.: Dynamics of bubble growth and detachment from a needle. *J. Fluid Mech.* **257**, 111–145 (1993)
5. Unverdi, S.O., Tryggvason, G.: A front-tracking method for viscous, incompressible, multi-fluid flows. *J. Comput. Phys.* **100**, 25–37 (1992)
6. Noh, W.F., Woodward, P.: SLIC (simple line interface calculation). In: *Proceedings of the Fifth International Conference on Numerical Methods in Fluid Dynamics*, June 28–July 2, 1976, Twente University, Enschede, Springer, pp. 330–340 (1976)
7. Hirt, C.W., Nichols, B.D.: Volume of fluid (VOF) method for the dynamics of free boundaries. *J. Comput. Phys.* **39**, 201–225 (1981)
8. Youngs, D.L.: Time-dependent multi-material flow with large fluid distortion. *Numer. Methods Fluid Dyn.* **24**, 273–285 (1982)
9. Ubbink, O.: Numerical prediction of two fluid systems with sharp interfaces. PhD Thesis, University of London (1997)
10. Weller, H.: A new approach to VOF-based interface capturing methods for incompressible and compressible flow. OpenCFD Ltd., Report TR/HGW/04 (2008)
11. Albadawi, A., Donoghue, D., Robinson, A., Murray, D., Delaure, Y.: Influence of surface tension implementation in volume of fluid and coupled volume of fluid with level set methods for bubble growth and detachment. *Int. J. Multiph. Flow* **53**, 11–28 (2013)
12. Sussman, M., Smereka, P., Osher, S.: A level set approach for computing solutions to incompressible two-phase flow. *J. Comput. Phys.* **114**, 146–159 (1994)
13. van Sint Annaland, M., Deen, N., Kuipers, J.: Numerical simulation of gas bubbles behaviour using a three-dimensional volume of fluid method. *Chem. Eng. Sci.* **60**, 2999–3011 (2005)
14. Chakraborty, I., Biswas, G., Ghoshdastidar, P.: A coupled level-set and volume-of-fluid method for the buoyant rise of gas bubbles in liquids. *Int. J. Heat Mass Transf.* **58**, 240–259 (2013)

15. Albadawi, A., Donoghue, D., Robinson, A., Murray, D., Delaure, Y.: On the analysis of bubble growth and detachment at low capillary and bond numbers using volume of fluid and level set methods. *Chem. Eng. Sci.* **90**, 77–91 (2013)
16. Li, Y., Yang, G., Zhang, J., Fan, L.-S.: Numerical studies of bubble formation dynamics in gas-liquid-solid fluidization at high pressures. *Powder Technol.* **116**, 246–260 (2001)
17. Valencia, A., Cordova, M., Ortega, J.: Numerical simulation of gas bubbles formation at a submerged orifice in a liquid. *Int. Commun. Heat Mass Transf.* **29**, 821–830 (2002)
18. Ma, D., Liu, M., Zu, Y., Tang, C.: Two-dimensional volume of fluid simulation studies on single bubble formation and dynamics in bubble columns. *Chem. Eng. Sci.* **72**, 61–77 (2012)
19. Osher, S., Sethian, J.A.: Fronts propagating with curvature-dependent speed: algorithms based on Hamilton–Jacobi formulations. *J. Comput. Phys.* **79**, 12–49 (1988)
20. Gollakota, A.R., Kishore, N.: CFD study on rise and deformation characteristics of buoyancy-driven spheroid bubbles in stagnant Carreau model non-Newtonian fluids. *Theoret. Comput. Fluid Dyn.* **32**, 35–46 (2018)
21. Chen, Y., Mertz, R., Kulenovic, R.: Numerical simulation of bubble formation on orifice plates with a moving contact line. *Int. J. Multiph. Flow* **35**, 66–77 (2009)
22. Sussman, M., Puckett, E.G.: A coupled level set and volume-of-fluid method for computing 3D and axisymmetric incompressible two-phase flows. *J. Comput. Phys.* **162**, 301–337 (2000)
23. Buwa, V.V., Gerlach, D., Durst, F., Schlücker, E.: Numerical simulations of bubble formation on submerged orifices: period-1 and period-2 bubbling regimes. *Chem. Eng. Sci.* **62**, 7119–7132 (2007)
24. Lafaurie, B., Nardone, C., Scardovelli, R., Zaleski, S., Zanetti, G.: Modelling merging and fragmentation in multiphase flows with SURFER. *J. Comput. Phys.* **113**, 134–147 (1994)
25. Georgoulas, A., Koukouvini, P., Gavaises, M., Marengo, M.: Numerical investigation of quasi-static bubble growth and detachment from submerged orifices in isothermal liquid pools: the effect of varying fluid properties and gravity levels. *Int. J. Multiph. Flow* **74**, 59–78 (2015)
26. Wu, W., Liu, Y., Zhang, A.: Numerical investigation of 3D bubble growth and detachment. *Ocean Eng.* **138**, 86–104 (2017)
27. Ghosh, A.K., Ulbrecht, J.: Bubble formation from a sparger in polymer solutions—I. Stagnant liquid. *Chem. Eng. Sci.* **44**, 957–968 (1989)
28. Terasaka, K., Tsuge, H.: Bubble formation at a single orifice in non-Newtonian liquids. *Chem. Eng. Sci.* **46**, 85–93 (1991)
29. Li, H.Z.: Bubbles in non-Newtonian fluids: formation, interactions and coalescence. *Chem. Eng. Sci.* **54**, 2247–2254 (1999)
30. Carreau, P.J.: Rheological equations from molecular network theories. *Trans. Soc. Rheol.* **16**, 99–127 (1972)
31. Berberović, E., van Hinsberg, N.P., Jakirlić, S., Roisman, I.V., Tropea, C.: Drop impact onto a liquid layer of finite thickness: dynamics of the cavity evolution. *Phys. Rev. E* **79**, 036306 (2009)
32. Brackbill, J., Kothe, D.B., Zemach, C.: A continuum method for modeling surface tension. *J. Comput. Phys.* **100**, 335–354 (1992)
33. Hoang, D.A., van Steijn, V., Portela, L.M., Kreutzer, M.T., Kleijn, C.R.: Benchmark numerical simulations of segmented two-phase flows in microchannels using the Volume of Fluid method. *Comput. Fluids* **86**, 28–36 (2013)
34. Gopala, V.R., van Wachem, B.G.: Volume of fluid methods for immiscible-fluid and free-surface flows. *Chem. Eng. J.* **141**, 204–221 (2008)
35. Van Leer, B.: Towards the ultimate conservative difference scheme. V. A second-order sequel to Godunov’s method. *J. Comput. Phys.* **32**, 101–136 (1979)
36. Rusche, H.: Computational fluid dynamics of dispersed two-phase flows at high phase fractions. Imperial College London (University of London) (2003)
37. Gerlach, D., Alleborn, N., Buwa, V., Durst, F.: Numerical simulation of periodic bubble formation at a submerged orifice with constant gas flow rate. *Chem. Eng. Sci.* **62**, 2109–2125 (2007)
38. Brackbill, J.U., Kothe, D.B., Zemach, C.: A continuum method for modeling surface tension. *J. Comput. Phys.* **100**, 335–354 (1992)
39. Simmons, J.A., Sprittles, J.E., Shikhmurzaev, Y.D.: The formation of a bubble from a submerged orifice. *Eur. J. Mech.-B/Fluids* **53**, 24–36 (2015)
40. Islam, M.T., Ganesan, P.B., Sahu, J.N., Sandaran, S.C.: Effect of orifice size and bond number on bubble formation characteristics: a CFD study. *Can. J. Chem. Eng.* **93**, 1869–1879 (2015)
41. Gerlach, D., Biswas, G., Durst, F., Kolobaric, V.: Quasi-static bubble formation on submerged orifices. *Int. J. Heat Mass Transf.* **48**, 425–438 (2005)
42. Di Bari, S., Lakehal, D., Robinson, A.: A numerical study of quasi-static gas injected bubble growth: some aspects of gravity. *Int. J. Heat Mass Transf.* **64**, 468–482 (2013)
43. Thoroddsen, S., Etoh, T., Takehara, K.: Experiments on bubble pinch-off. *Phys. Fluids* **19**, 042101 (2007)
44. Gordillo, J., Sevilla, A., Rodríguez-Rodríguez, J., Martínez-Bazan, C.: Axisymmetric bubble pinch-off at high Reynolds numbers. *Phys. Rev. Lett.* **95**, 194501 (2005)
45. Burton, J., Waldrep, R., Taborek, P.: Scaling and instabilities in bubble pinch-off. *Phys. Rev. Lett.* **94**, 184502 (2005)
46. Bhaga, D., Weber, M.: Bubbles in viscous liquids: shapes, wakes and velocities. *J. Fluid Mech.* **105**, 61–85 (1981)